HHS Public Access

Author manuscript

Nat Mater. Author manuscript; available in PMC 2016 May 18.

Published in final edited form as:

Nat Mater. 2015 December ; 14(12): 1278–1285. doi:10.1038/nmat4422.

A Sunblock Based On Bioadhesive Nanoparticles

Yang Deng[1,†], **Asiri Ediriwickrema**[1,†], **Fan Yang**[1], **Julia Lewis**[2], **Michael Girardi**[2], and **W. Mark Saltzman**[1]

W. Mark Saltzman: mark.saltzman@yale.edu

[1]Department of Biomedical Engineering, Yale University, 55 Prospect Street, New Haven, CT 06511, USA

[2]Department of Dermatology, Yale University, 333 Cedar Street, New Haven, CT 06520, USA

Abstract

The majority of commercial sunblock preparations utilize organic or inorganic ultraviolet (UV) filters. Despite protecting against cutaneous phototoxicity, direct cellular exposure to UV filters has raised a variety of health concerns. Here, we show that the encapsulation of padimate O (PO) - a model UV filter - in bioadhesive nanoparticles (BNPs) prevents epidermal cellular exposure to UV filters while enhancing UV protection. BNPs are readily suspended in water, facilitate adherence to the stratum corneum without subsequent intra-epidermal or follicular penetration, and their interaction with skin is water-resistant yet the particles can be removed via active towel drying. Although the sunblock based on BNPs contained less than 5 wt% of the UV-filter concentration found in commercial standards, the anti-UV effect was comparable when tested in two murine models. Moreover, the BNP-based sunblock significantly reduced double-stranded DNA breaks when compared to a commercial sunscreen formulation.

Ultraviolet (UV) radiation from sunlight can lead to multiple adverse effects including cutaneous phototoxicity (sunburn), photoaging, and carcinogenesis[1–6]. UVB directly induces cyclopyrimidine dimers (CPDs) within the genomic DNA (gDNA) of keratinocytes and melanocytes, and both UVA and UVB exposure markedly enhance production of reactive oxygen species (ROS) that damage a variety of cellular components, including gDNA[7, 8], and induce immunosuppressive cytokines. Thus, it is not surprising that UV-exposure is clearly linked to both melanoma and non-melanoma skin cancer development[9–11].

Epidemiologic studies have shown that there is a greater incidence and risk of developing melanoma and non-melanoma skin cancer with increased ambient UV exposure and cutaneous sun sensitivity[12]. Over the past few decades, commercially available UV-

Correspondence to: W. Mark Saltzman, mark.saltzman@yale.edu.

†Y.D. and A.E. contributed equally to this work

AUTHORS' CONTRIBUTION

Y.D., A.E., J. L., F.Y., M. G. and W.M.S. designed the experiments. Y.D., A.E., F.Y. and J. L. performed the experiments. All the authors were involved in the analyses and interpretation of data. Y.D., A.E., M.G. and W.M.S. wrote the paper, with the help of the co-authors.

protective sunblocks have largely incorporated organic UV filters [e.g. avobenzone, octinoxate, octocrylene, oxybenzone and padimate O (PO)[13]] as formulations based on oil/water emulsions[14]. There are substantial concerns, however, that these aromatic organic compounds can penetrate through the stratum corneum, or via follicles, into epidermal cells, including keratinocytes and Langerhans cells[13, 15]. The potential for systemic absorption of such organic compounds, and their depot in adipose tissue, has also been a concern[8, 16–18] (Fig. 1). Moreover, several UV filters have been detected in human urine and breast milk samples after topical treatment, and may mediate systemic effects including endocrine disruption[13, 18, 19]. Therefore, minimizing direct skin contact and subsequent epidermal penetration may be essential to eliminating the potential adverse effects of sunscreens.

Alternatively, UV-blocking inorganic materials such as micronized zinc oxide (ZnO) and titanium dioxide (TiO_2) particles[20] have been utilized. While transdermal penetration of the inorganic particles appears to be less of a concern than for the organic agents[21], both types of sunblock agents have shown the capacity to enhance ROS generation after UV exposure, suggesting that even small quantities may contribute to cellular damage and ultimately carcinogenesis[22–25]. Thus, while the application of such products protects against sunburn, e.g. raises the skin's minimal erythema dose (MED), there continues to be controversy regarding their overall effectiveness in preventing skin cancer[18, 26–28].

Additionally, commercial sunscreens based on micronized ZnO and TiO2 are opaque, due to their large particle size. Nanoparticles, of the size used in this study, yield more transparent suspensions, which may be favored in topical applications for aesthetic reasons. Paradoxically, such smaller inorganic nanoparticles currently used in commercially available sunscreens may accumulate in hair follicles or penetrate deep into the dermis to cause a variety of adverse effects[29, 30]. Numerical simulations of nanoparticle properties suggest that unless small nanoparticles can be clearly demonstrated as safe, it is increasingly difficult to solve this paradox[20]. Here we address this problem by utilizing nanoparticles with bioadhesive properties to prevent nanoparticle deposition into hair follicles. This strategy may also be useful in other topical applications[31, 32]. In this study, we demonstrate that sunblock based on bioadhesive nanoparticles (BNPs) encapsulating PO is not only persistently adherent and non-penetrant, but also is highly preventive against primary UV-induced damage as well as secondary ROS toxicity. Recently, we reported on polylactic acid-hyperbranched polyglycerol (PLA-HPG) nanoparticles or non-bioadhesive nanoparticles (NNPs) that provide for enhanced circulation times and drug delivery into solid tumors.[33] Here, we modified these nanoparticles by converting the HPG into an aldehyde rich corona, which provides an unprecedented bioadhesive property. Aldehydes readily form a variety of linkages with proteins, such as Schiff-base linkages with primary amines on proteins[34], and thus are commonly used as fixation reagents for histological studies[35], surface coatings to immobilize proteins on microarray surfaces[36], and bioadhesives for wound healing[37].

We hypothesized that the bioadhesive properties of aldehyde-terminated nanoparticles would allow for improved particle retention in topical applications, thereby inhibiting primary and secondary UV-mediated toxicity. Our results show that BNPs remain on the stratum corneum after topical application without penetration into the cellular epidermis or dermis.

In contrast, similar sized NNPs were observed to penetrate deep into the hair follicles. The interaction between BNPs and skin is water-resistant but the BNPs are readily removed with active towel drying. Additionally, topical BNPs were removed by the physiologic regeneration of the stratum corneum over the course of several days. Notably, PO encapsulation in BNPs enhanced the UV absorbance of PO by 20-fold relative to free PO suspended in water, and significantly reduced UV filter release and ROS mediated toxicity in adjacent tissue. Our BNP formulation, comprising less than 5% (by weight) of the UV filter concentration found in commercial standards, was comparable to commercially available sunscreen in protecting against sunburn in murine models. Further, the BNP sunscreen significantly lowered the level of DSBs when compared to commercial sunscreen.

Previously, we developed HPG coated core-shell NNPs and evaluated their non-adherent properties in detail[33]. Because the HPG coating is rich in vicinal diols, NNPs can be readily oxidized to aldehyde-terminated BNPs by sodium periodate ($NaIO_4$) treatment. This was validated by H^1NMR (Fig. S1) and Schiff's agent (data not shown) analysis. The surface density of aldehydes on BNPs was monitored as a function of incubation time with $NaIO_4$ and it reached its saturation in ~20 min (Fig. 2A). The final surface density of aldehydes on BNPs approached 9/nm^2 (17 aldehydes/PLA molecule), indicating that the majority of surface vicinal diols were converted to aldehydes. This surface density of functional groups is at least one order of magnitude higher than previously reported on biodegradable nanoparticles[38]. Moreover, the surface density of the aldehydes can be controlled by incubation time with $NaIO_4$. No detrimental effects of aldehyde conversion were observed on nanoparticles by TEM imaging (Fig. S2A). The average diameter of nanoparticles was approximately 96 nm as measured by dynamic light scattering (DLS) (Table S1).

We investigated the bioadhesive properties of the BNPs using poly-L-lysine (PLL) coated glass slides[39]. The multiple amine groups on PLL mimic the amines present on extracellular proteins on the epidermis, and provide potential targets for particle adhesion. BNPs with different concentrations of aldehyde were prepared and printed onto poly-L-lysine coated slides with a microarrayer. The non-treated nanoparticle group (NNP, with 0 min of exposure to $NaIO_4$,) did not adhere to PLL-coated glass slides (Fig. 2B). However, after oxidizing surface HPG vicinal diols on NNPs into aldehydes with $NaIO_4$, the amount of BNPs immobilized on the glass slide increased as a function of $NaIO_4$ treatment duration (Fig. 2B), indicating that the bioadhesive property of the BNPs increases with a longer duration of $NaIO_4$ treatment. Moreover, the large capacity for surface aldehyde modification allows for tuning adhesiveness for specific topical applications. To better understand the mechanism for surface adherence, we used formaldehyde, which readily forms Schiff-base bonds with amine groups on lysine side chains[34], to block the free amines on the lysine residues. Because of the reversibility of the Schiff-base, formaldehyde was also added into the PBS solution containing NPs. Our results showed no adhesion of BNPs co-treated with formaldehyde on PLL-coated surfaces. The difference was clearly visualized by the absence of fluorescence on the glass slides (Fig. S3). This result suggests that particle adhesion on PLL-coated slides is due to Schiff-base linkages with amine groups on the surface lysine molecules.

Ideal vehicles for UV-filters should only remain on the skin surface, without penetration into the epidermis, dermis, or hair follicles, in order to avoid potential health risks[18]. Thus, we compared the *ex vivo* retention and penetration of BNPs and NNPs by applying suspended particles topically onto pig skin. We considered pig skin a reasonable mimic for human skin, as it has been examined in a variety of topical applications including penetration studies for chemicals and nanoparticles[4041]. In prior work, we have shown that these NNPs resist non-specific interaction with a variety of biomolecules, and provide a comparable non-adhesive control[33]. To facilitate imaging and quantification, both NNPs and BNPs were loaded with a hydrophobic dye, 0.2%1,1'1'-dioctadecyl-3,3,3',3' –tetramethylindodicarbocyanine,4-chlorobenzenesulfonate salt (DiD)[33]. Both the DiD/NNPs and DiD/BNPs were characterized by TEM (Fig. S2B, C) and DLS (Table S1), and had a similar spherical morphology and DiD loading (0.2%). After a 6 hour incubation on pig skin followed by washing with PBS, BNPs showed substantially higher skin retention compared to NNPs (Fig. 2C, D). There was no observed penetration of BNPs in these skin samples; in contrast, we found that NNPs penetrated into follicles without significant retention on the stratum corneum (Fig. S4). These results suggest that adhesion of BNPs to skin surface proteins prevents their subsequent penetration of skin and deposition within follicles.

To better understand the mechanism for surface adherence of BNPs on pig skin, we again used formaldehyde, which readily reacts with protein in tissues with a variety of bonds[34], including Schiff-base bonds, to compete against interactions with surface aldehydes on BNPs. Because of the reversibility of the bonds between formaldehyde and proteins[34], formaldehyde was also added into the PBS solution of BNPs. Our results showed that the adhesion of BNPs co-treated with formaldehyde was significantly lower than BNPs not treated with formaldehyde (Fig. S5). This supports that the adhesion of BNPs on pig skin is due to the interaction of its outer aldehyde residues with skin surface proteins.

We also evaluated the water resistance and potential for removal of BNPs by encapsulating an infrared dye, IR-780, into BNPs (0.5% loading), and measuring nanoparticle skin concentrations with *in vivo* imaging. The IR-780/BNPs were characterized by TEM (Fig. S2D) and DLS (Table S1). We applied the IR-780/BNPs topically onto nude mice. After washing with continuous water irrigation for one minute, no significant change in fluorescence was observed; however, the BNPs were removed after wiping with a wet towel (Fig. 2G, H). If untreated, BNP concentration diminished markedly (~75%) within 24 hours. Particle disappearance from the skin was essentially complete after five days (Fig. 2E, F), which coincides with the stratum corneum turnover time for hairless mice[42]. BNPs may be ideal vehicles for sunscreen application since they are water-soluble but their interaction with skin is water-resistant. The BNPs disengage from skin naturally by exfoliation of the stratum corneum; removal can be accelerated mechanically by towel wiping. Commercial sunscreens polymerize monomers with an initiator or use film forming polymers in order to stabilize the UV filters onto the skin. The chemicals involved include a variety of acrylate derivatives and multiple initiators[43], which have been implicated in irritant and allergic contact dermatitis[44, 45]. Sunscreens based on BNPs simplify the current sunscreen formulation as well as eliminate the use of irritants and/or allergens.

The ideal UV-filter for our system should have hydrophobic properties for easy particle encapsulation and a high UV absorbance. PO has favorable hydrophobic properties and a high extinction coefficient when compared to other commercial UV filters[46]; therefore, PO was used as our candidate UV filter for evaluating the effectiveness of BNPs as sunblock. All PO encapsulated BNPs used in these studies contained 10% PO (PO/BNPs). The spherical shape of the PO/BNPs was confirmed by TEM (Fig. 3A). The average hydrodynamic diameter of PO/BNPs was 138 nm as measured by DLS (Table S1). The stability of PO encapsulation in nanoparticles was evaluated by measuring the release of PO in artificial human sweat. After 24 hours, PO/BNPs released only 2.9% and 4.0% of the total PO load at 32 °C and 37 °C respectively (Fig. 3B). We also investigated the skin penetration of PO after treatment with PO encapsulated nanoparticles; PO dissolved in mineral oil (PO/oil) was used as a positive control[13]. After a 6 hour treatment, the skin specimens were washed and tape stripped to remove residual surface material, and PO was extracted from the skin and quantified with HPLC. PO levels measured in tape stripped skin after PO/BNPs treatment were indistinguishable from background (PBS control) suggesting that no PO penetrated into the skin. On the other hand, the PO level measured in tape stripped skin after PO/NNP treatment is above background; however, it is lower than the PO/oil control, suggesting minimal penetration of PO from PO/NNPs (Fig. S6). Encapsulating UV filters within BNPs will result in minimal epidermal cellular exposure and, therefore, should decrease associated toxicity.

We investigated the long-term toxicity of BNPs. PO/BNPs, blank BNPs and PBS were applied to dorsal mouse skin every other day for a total of six applications. Afterwards, skin treated with PO/BNPs and blank BNPs were indistinguishable from the PBS control. In all samples, there was no histologic evidence of cutaneous irritancy, toxicity or inflammation (Fig S7). Specifically, the epidermis appeared unperturbed with a normal basket weave stratum corneum and normal thickness. The dermis also appeared normal without any inflammatory infiltrates. Skin follicles and sebaceous structures appeared normal in all samples as well.

Most organic UV filters prevent sunburn by absorbing UV radiation. Therefore, their effectiveness can be estimated by measuring their UV absorption efficiency. We evaluated the UV absorption of PO/BNPs by measuring their absorption spectrum within the UV range (260–400 nm). PO/BNPs were compared to PO emulsified in water (PO/water), PO/oil, PO dissolved in dimethyl sulfoxide (PO/DMSO), sunscreen (L'Oréal sunscreen oil spray) in mineral oil (sunscreen/oil); blank BNPs, mineral oil, DMSO and water were used as controls (Fig. 3C). All solutions containing PO had a concentration of PO at 0.01mg/ml and the sunscreen/oil solution had a concentration of active ingredient at 0.01mg/ml. PO/BNPs showed a 20-fold higher absorption when compared to PO emulsified in water and sunscreen dissolved in oil after background subtraction of the appropriate base material. The PO/water emulsion is a simplified, representative version of a sunscreen formulation[47], as most current sunscreens are based on the emulsion of UV filters[48]. The sunscreen oil used here is an oil spray with the same active ingredients and sun protection factor (SPF) value as the sunscreen lotion used in our animal studies. Moreover, PO/BNPs showed a much higher and broader absorption compared to PO dissolved in mineral oil. The PO dissolved in mineral oil is a representative version of traditional sunscreen oil[13]. These results indicate a significant

improvement in UV absorption efficiency of PO/BNPs compared to other formulations or commercial sunscreens which is perhaps due to the improved solubility of PO within the BNP carrier. We also compared the UV absorption of PO/BNPs to that of PO dissolved in DMSO. The UV absorbance of PO/BNPs is about 1.5 times that of the PO/DMSO after background subtraction. We believe this is due to the enhanced scattering resulting from the size difference of BNPs and PO/BNPs (Table S1). We used the blank BNPs as background for PO/BNPs but the size of PO/BNPs increased 44% compared to blank BNPs[49].

Photoinduced changes in UV filters often produce toxic intermediates including ROS that are destructive to multiple cellular components including gDNA[8]. It has been reported that encapsulating UV filters in polymeric nanoparticles improves filter photostability and delays photodegradation of the UV filters[50]. Therefore, we hypothesize that encapsulating UV-filters into BNPs will confine any generated ROS within the nanoparticles and eliminate potential side-effects. Dihydrorhodamine (DHR), a widely utilized ROS probe[8], was used to detect reactive radicals generated by PO after UV exposure. DHR was mixed with PO/BNPs, emulsified PO, and BNPs separately and exposed to UV radiation. DHR in PBS was used as a control because it absorbs UV at 280–315 nm and becomes fluorescent. The BNPs had a negligible effect on the background fluorescence of DHR as measured by the control since they did not absorb UV. The fluorescence from the PO suspension is much higher than the control (Fig. 3D). We believe that the free ROS generated from the photoactivated PO oxidized the DHR into fluorescent species. In contrast, by confining the ROS within nanoparticles, the photoactivated PO in PO/BNPs has no effect on DHR. In addition, PO adsorbs part of the UV irradiation while inside BNPs, and, therefore, DHR in the PO/BNP group was exposed to less UV resulting in lower background fluorescence.

We initially evaluated the protective effects of PO/BNPs against sunburn on nude mouse skin. The dorsal skin of each mouse was divided into four quadrants receiving either PO/BNPs, sunscreen, blank BNPs, or PBS. The skin was subsequently exposed to UVB and UVA (280–400 nm) at a high dose, 2160J/m^2. Three days after UV exposure, skin treated with both PO/BNPs and sunscreen contained no visible erythema, edema or ulceration. However, both skin patches treated with PBS and blank BNPs were damaged considerably by the same UV exposure (Fig. S8). A similar pattern of UV toxicity was seen after staining the dorsal skin with hematoxylin and eosin (H&E) (Fig. 4A, C, E, G, I and K). There was significant acanthosis with prominent rete ridges present in the unprotected samples, consistent with epidermal hypertrophy, whereas the skin protected by sunscreen or PO/BNPs appeared comparable to normal controls. The UV filter concentration in PO/BNPs was less than 5% of that contained in the sunscreen, yet the PO/BNPs achieved a similar gross UV protection effect. Trichrome staining was also employed to measure the anti-UV effect against sunburn (Fig. 4B, D, F, H, J and L). Interestingly, skin protected by sunscreen showed thickened orthokeratosis, a more subtle epidermal response to UV-damage, relative to the skin protected by PO/BNPs and the normal skin control. Overproduction of keratin can cause keratosis pilaris, often blocking the opening of hair follicles and resulting in further skin irritation. These results may therefore demonstrate another non-irritating advantage of BNP based sunblock.

UVB irradiation can directly excite nucleobases resulting in the formation of cyclobutane pyrimidine dimers (CPDs). The accumulation of CPDs within the gDNA can lead to apoptosis, mutagenesis, and potentially carcinogenesis[51]. We evaluated PO/BNPs in a second animal model to further understand their anti-UV effects against CPD formation. Mice were exposed to UVB (160 J/m^2, 280–320 nm) and the formation of CPDs was visualized with immunostaining. Both PO/BNPs and sunscreen showed no detectable CPDs, but both the positive control (unprotected skin) and the PO/NNPs revealed marked widespread CPD formation after UV exposure (Fig. 5A, B). Again, even though UV filter content in PO/BNPs was less than 5% of that in the control sunscreen, it achieved the same level of UV protection. Additionally, UV irradiation can produce DSBs, which are highly carcinogenic. UVB exposure does not directly produce DSBs; however, it is possible that UV filters present in the epidermis and dermis can produce ROS after photoactivation, react with cellular DNA, and ultimately produce DSBs[8, 16, 17, 52]. DSBs recruit phosphorylated histone H2A variant H2AX (γH2AX) to the damaged sites[53]. The group of mice treated with conventional sunscreen showed the highest level of DNA-damage by γH2AX recruitment. In contrast, the level of γH2AX in the PO/BNPs, no protection, and non UV exposed sunscreen treatment groups were comparable to the normal skin control (Fig. 6A, B).

UV exposure from sunlight remains a significant health risk, and there continues to be controversy as to the safety and benefits of commercially available sunscreens. In order to address these issues, we developed a sunblock based on BNPs. Relative to a conventional preparations, the BNP sunblock demonstrated a durable and specific adherence to the stratum corneum, without any evidence of penetration into cellular components of the epidermis; a 20-fold greater UV spectral absorbance; superior protection against UV-induced CPDs and DSBs; and improved protection against UV-induced orthokeratosis. Additionally, BNPs on skin are water resistant, yet are easily removed with towel wiping, or disappear naturally by exfoliation of the stratum corneum. Encapsulating UV filters within BNPs prevented skin exposure to the filter molecules, and the subsequent ROS produced after UV photochemical activation. With less than 5% of UV filters in commercial standards, the protective effect of PO/BNPs against sunburn was comparable to commercial sunscreen in animal studies, and had the added benefit of preventing subsequent ROS mediated DSBs.

Material and Methods

IR-780 iodide, glycerol, NaIO4 and *Bovine serum albumin* (BSA) were obtained from the Sigma-Aldrich. The 1,1'-Dioctadecyl-3,3,3',3'-Tetramethylindodicarbocyanine,4 Chlorobenzenesulfonate Salt (DiD) and 4,6-diamidino-2 phenylindole (DAPI) stain were ordered from Invitrogen. Aldehyde Quantification Assay Kit (Fluorometric) was from Abcam. Poly -L -lysine coated glass slides were obtained from VWR International Inc..Walgreens sunscreen lotion (SPF 30,, Avobenzone 3.0%, Homosalate 10.0%, Octisalate 5.0%, Octocrylene 10%) was purchased from Walgreens. Sunscreen oil (SPF 30, Avobenzone 3.0%, Homosalate 10.0%, Octisalate 5.0%, Octocrylene 7%) was from L'Oréal Paris.

Synthesis and characterization of BNPs

NNPs were converted into BNPs by $NaIO_4$ treatment. Briefly, one volume of NNPs at 25mg/ml was incubated with three volume of $NaIO_4$ at 0.1M in the presence of one volume of 10× PBS for 20 min and then the reaction was quenched with three volume of Na_2SO_3 0.2M. The nanoparticles were washed two times with DI water in Amicon filters with 100k cut-off and then resuspended in DI water. To quantitatively study the conversion of vicinal diols on NNPs to aldehydes with $NaIO_4$ treatment, NNPs (0.1 mg/ml) in PBS were incubated with 1mM $NaIO_4$ and at each time point, the reactions were quenched with 2mM Na_2SO_3. The nanoparticles were washed two times with DI water in Amicon filters with 100k cut-off and then resuspended in DI water. The aldehydes on nanoparticles were quantified with an aldehyde quantification assay kit (Abcam). The NNPs were used as a background subtraction control. The amount of aldehyde was calculated by comparing to a reference curve obtained using the aldehyde standards provided with the kit. The amount of aldehyde on each particle was calculated based on the 100 nm hydrodynamic diameter of nanoparticles and an assumed nanoparticle density of 1.0 g/cm^3.

Evaluation of particle adhesion *in vitro*

For microarray printing, BNPs loaded with 0.2% DiD dye were suspended in PBS buffer containing 15% glycerol and 0.01% triton-X100 at a concentration of 1 mg/ml in a 384-well plate. This protocol was modified from a protocol previously used to eliminate ring-effect in microarray printing[54]. Nanoparticles were arrayed on lysine coated slides using a Spotbot microrrayer from Arrayit. After a 1 hour incubation in a humidity chamber, the printed slides were washed with PBS three times for five minutes on an orbital shaker[55]. After a quick rinse with DI water, the slides were blow-dried with argon and imaged with an Evos microscope. The fluorescence was quantified with ImageJ software. To study BNP adhesion onto formaldehyde pretreated slides, lysine coated protein slides were divided into blocks with a pap pen. PBS or PBS with 2% formaldehyde was added individually to the blocks. After incubation for 15 min, the solution was aspirated and the slides were dried with argon. Subsequently, BNPs loaded with 0.2% DiD dye (DiD/BNPs) suspended in PBS buffer containing 15% glycerol and 0.01% triton-X100 at a concentration of 1 mg/ml were arrayed on the blocks pretreated with PBS. This group was compared to DiD/BNPs suspended in PBS buffer containing 15% glycerol, 0.01% triton-X100 and 2% formaldehyde at a concentration of 1 mg/ml which were similarly arrayed on the blocks pretreated with PBS containing 2% formaldehyde. With the same incubation and washing steps, the slides were blow-dried with argon and imaged with a microarray scanner. The fluorescence was quantified with ImageJ software.

Evaluation of BNP skin adhesion *ex vivo*

Fresh pig skin was obtained from a local slaughterhouse and the hair was carefully removed by a trimmer to ensure skin was not damaged. The skin was frozen at −20 °C, and thawed on ice before use. Thawed pig skin was washed with PBS buffer and cut into 2×2 cm pieces. Both the DiD/BNPs and DiD/NNPs in the following experiments had the same loading of DiD dye at 0.2%. For the fluorescence imaging experiment, DiD loaded NNPs and BNPs in PBS were applied topically to pig skins and incubated for 6 h in a humidity chamber at

32 °C. After incubation, each skin sample was washed topically with 20 ml PBS buffer for 3 times, 5 min each and frozen in OCT. The frozen skin was sectioned into 10–20 μm slices, mounted on glass slides, and imaged with an EVOS fluorescence microscope.

To further evaluate the mechanism for particle adhesion, PBS or PBS containing 2% formaldehyde was applied topically onto the skin samples, and aspirated 15 min later. DiD/BNPs at 1mg /ml in PBS containing 2% formaldehyde were applied topically onto pig skin samples pretreated with PBS (pH=7.4) containing 2% formaldehyde. DiD/BNPs at 1mg /ml in PBS were applied topically to pig skin samples pretreated with only PBS (pH=7.4). After incubation for 6 h in a humidity chamber at 32 °C, each skin sample was washed topically with 20 ml PBS buffer 3 times, for 5 min each and dried. Each skin sample was tape stripped 30 times and the NPs collected on tapes were dissolved with DMSO. DiD fluorescence was quantified by a plate reader.

Evaluation of BNP skin adhesion *in vivo*

All animal procedures were performed in accordance with Yale IACUC protocols. Animals were kept in the Yale Animal Resource Center and given free access to food and water over the duration of the study. For the live imaging study, the dorsal skin of each nude mouse was cleaned with an alcohol pad and 1 mg/ml of IR-780/BNPs (0.5%) in PBS was applied to the skin. The nanoparticles remaining on the skin were imaged by Xenogen. For evaluation of nanoparticle retention, the mice were housed individually and imaged at each time point. For evaluation of BNP water resistance and mechanical removal, one group of mice (n=3) was wiped with a wet towel and the other group of mice was washed with water. The mice were subsequently dried with kimwipes and sent for live imaging.

Synthesis and characterization of PO/BNPs

PLA-HPG polymer and PO at a certain ratio (total mass of 50–100 mg) were dissolved in a mixture of 2.4 ml ethyl acetate and 0.6 ml DMSO, which was subsequently added into 4 ml of DI water under vortexing and subjected to probe sonication for three cycles at 10 sec each. The resulting emulsion was diluted in 10ml DI water under stirring. The solution was hooked up to a ratovapor to evaporate the ethyl acetate and then applied to an Amico ultra centrifuge filtration unit (100k cut-off). The PO/NNPs nanoparticles were washed by filtration two times and then suspended in DI water. The same procedure was implemented to produce PO/BNPs, as NNPs were converted into BNPs as described earlier. To quantify the PO loading, the nanoparticles were dissolved in DMSO and the UV absorbance at 310 nm was measured with a plate reader. The amount of PO was calculated by comparing to a reference curve. To quantify PO release from nanoparticles, a suspension of 4 mg nanoparticles were loaded with PO in a dialysis tube (10K cut-off) and was dialyzed against 40ml of artificial sweat EN 1811 (0.5% NaCl, 0.1% urea, 0.1% lactic acid and the pH adjusted to 6.6 with NH4OH) at 32 °C and 37 °C. At each time point, 150 μL of solution was removed and 150 μL of fresh solution was added. The amount of PO released was quantified by UV absorption at 310 nm with a plate reader.

Evaluation of UV absorbance efficiency of PO/BNPs *in vitro*

PO/BNPs suspended in water, PO emulsified in water, PO dissolved in mineral oil (PO concentration at 0.01mg/ml) and sunscreen oil diluted in mineral oil (active ingredients adjusted to 0.01 mg/ml) were aliquoted into a UV transparent plate and scanned through the UV absorbance spectrum from 260–400 nm with a plate reader. Blank BNPs, water and mineral oil were also scanned as background controls. The PO emulsion in water was made by probe sonication. For the DHR assay, PO/BNPs, BNPs, PO water emulsion at a PO concentration of 0.1mg/ml was incubated with DHR in PBS buffer in 96 well plate. After exposing to UV-B (280–320 nm), plate fluorescence was read at Ex/Em 500/536 nm.

Evaluation of PO skin penetration from PO/BNPs *ex vivo*

Fresh pig skin was obtained from a local slaughterhouse and the hair was carefully removed by a trimmer to ensure skin was not damaged. The skin was frozen at −20 °C, and thawed on ice before use. Thawed pig skin was washed with PBS buffer and cut into 2×2 cm pieces. Both the PO/BNPs and PO/NNPs had the same loading of PO at 10%. For HPLC study, PO/BNPs in PBS, PO/NNPs in PBS, PO/mineral oil at PO concentration of 1mg/ml, and PBS were applied topically onto skin samples. After incubation for 6 h in a humidity chamber at 32 °C, each skin sample was washed topically 3 times with 20 ml PBS buffer, 5 min each and dried. Each skin sample was tape stripped 30 times and then wiped with alcohol swabs 3 times. Each specimen was chopped and PO was extracted with 4 ml acetonitrile. The PO concentration was determined with HPLC on C18 column with acetonitrile/water (9:1) at 310 nm absorbance.

Long term toxicity of PO/BNPs *in vivo*

All animal procedures were performed in accordance with Yale IACUC protocols. Animals were kept in the Yale Animal Resource Center and given free access to food and water over the duration of the study. The dorsal hair of FVB/NJ mice was shaved with electric clippers and treated with depilatory cream. Three days later, the mice were single caged, divided into 3 groups, and received either PO/BNPs, blank BNPS or PBS every other day for six total applications. Three days after the final application, duplicate 4 × 30 mm skin strips were harvested from the treated dorsal skin of each mouse (n=3 PBS, n=4 blank BNP, n=4 PO/BNP) for histologic examination. Formalin fixed paraffin embedded samples were prepared, stained with H&E and examined by a dermatologist blinded to the experimental groups using a Zeiss Axio Observer Z1 microscope. Images were collected using TissueGnostics TissueFAX software and Baumer Optronic HXG40c camera.

Anti-UV evaluation of PO/BNPs *in vivo*

Walgreens sunscreen lotion was used in all of the *in vivo* experiments. All animal procedures were performed in accordance with Yale IACUC protocols. Animals were kept in the Yale Animal Resource Center and given free access to food and water over the duration of the study. For our first *in vivo* experiment, nude mice were anesthetized with Ketamine/Xylazine, and their dorsal skin was cleaned with 70% alcohol and demarcated into four quadrants. One quadrant was used as a PBS control and other areas were treated with sunscreen, PO/BNPs or blank BNPs. Only the dorsal epidermis was exposed to the UV lamp

(UV-B, 8W) for one min (2160J/m^2) and the remaining skin was covered with screens. The mice were left in separate cages and monitored until they woke up. Three days after UV exposure, the dorsal skin was removed and prepared for histology. Images were analyzed for epidermal thickness and keratin content using ImageJ (NIH).

For our second *in vivo* experiment, the dorsal hair of FVB mice was shaved with electric clippers and treated with depilatory cream. One week later, the mice received either PO/BNPs, PO/NNPs, sunscreen, or no treatment followed by dorsal exposure to UV (160 J/m^2) one hour after treatment. For CPD staining, dorsal skin flaps were removed five minutes after UV exposure, and incubated in PBS containing 20 mM EDTA for 2 hours at 37°C to allow separation of the epidermis from the dermis. The epidermal sheet was then rinsed in PBS, fixed in acetone for 20 min at −20°C, then permeabilized in cold PBS containing 0.5% Triton X-100 for 30 min. Sheets were denatured with 0.4 M NaOH in 70% ethanol for 22 min and then washed with cold PBS containing 0.5% Triton X-100 four times, eight min each. Sheets were blocked with PBS containing 2% BSA, 0.5% Triton-X-100 and 1% goat serum for one hour at room temp, then stained overnight at 4°C with anti-thymine dimer (2 mg/ml, Abcam#ab10347) diluted in PBS containing 0.4% BSA and 0.5% Triton X-100. The remaining steps were carried out at room temperature. Samples were washed in PBS containing 0.5% Triton-X 100 for two hours, stained for two hours with Alexa568-goat-anti-mouse IgG (Invitrogen), washed again, mounted in DAPI (Invitrogen) and examined under a Leica 5P Confocal microscope. For γH2AX staining, 20 hours after UV exposure, dorsal skin flaps were removed and incubated in 0.5 M ammonium thiocyanate for 20 min at 37°C to allow for separation of the epidermis from the dermis. The epidermal sheet was then rinsed in PBS, fixed in acetone for 20 min at −20°C, then rehydrated in cold PBS. Sheets were blocked and nuclei were permeabilized in PBS containing 2% BSA and 0.5% Triton-X-100 for one hour at room temp, then stained overnight at 4°C with anti-γH2AX (1 mg/ml, clone JBW30, Millipore, Billerica, MA) diluted in PBS containing 0.4% BSA and 0.5% Triton X-100. The remaining steps were carried out at room temperature. Samples were washed in PBS containing 0.5% Triton-X 100 for two hour, stained for two hour with Alexa568-goat-anti-mouse IgG (Invitrogen), washed again, mounted in DAPI (Invitrogen) and examined under a Leica 5P Confocal microscope. For CPD staining, 5 fields/sheet (1 sheet/mouse) were taken using the stage control to move 1 mm between fields in a set pattern. The fluorescence from CPD staining on nuclei was quantified by image J. For γH2AX staining, all of the areas with γH2AX+ cells on a sheet (1 sheet / mouse) were imaged. The γH2AX+ cells were counted using ImageJ (NIH) particle analyzer software with the threshold set to eliminate background γH2AX staining. The surface concentration of γH2AX+ cells was calculated by dividing the overall number of the γH2AX+ cells on a sheet with the surface area of the sheet.

Supplementary Material

Refer to Web version on PubMed Central for supplementary material.

Acknowledgements

We are grateful to Yu Wu, Yao Lu, Rong Fan, Yukun Pan, Tian Xu and Themis Kyriakides of Yale University for access to their instruments in their laboratories. We thank Elias Quijano and Themis Kyriakides for helpful

discussions and Junwei Zhang for technical assistance. This work was supported by NIH grants CA102703, EB000487 and CA149128, Yale School of Medicine Office of Student Research, and the Howard Hughes Medical Research Fellowship.

References

1. Federman DG, Kirsner RS, Concato J. Sunscreen counseling by US physicians. Jama. 2014; 312:87–88. [PubMed: 25058222]
2. Stern RS. The risk of melanoma in association with long-term exposure to PUVA. Journal of the American Academy of Dermatology. 2001; 44:755–761. [PubMed: 11312420]
3. Lim JL, Stern RS. High levels of ultraviolet B exposure increase the risk of non-melanoma skin cancer in psoralen and ultraviolet A-treated patients. The Journal of investigative dermatology. 2005; 124:505–513. [PubMed: 15737190]
4. Bordeaux JS, Lu KQ, Cooper KD. Melanoma: prevention and early detection. Semin. Oncol. 2007; 34:460–466. [PubMed: 18083369]
5. Liu H, Tuchinda P, Fishelevich R, Harberts E, Gaspari AA. Human in vitro skin organ culture as a model system for evaluating DNA repair. J. Dermatol. Sci. 2014; 74:236–241. [PubMed: 24636351]
6. Eller MS, Asarch A, Gilchrest BA. Photoprotection in human skin--a multifaceted SOS response. Photochem. Photobiol. 2008; 84:339–349. [PubMed: 18179622]
7. Gilchrest BA. Photoaging. The Journal of investigative dermatology. 2013; 133:E2–E6. [PubMed: 23820721]
8. Hanson KM, Gratton E, Bardeen CJ. Sunscreen enhancement of UV-induced reactive oxygen species in the skin. Free radical biology & medicine. 2006; 41:1205–1212. [PubMed: 17015167]
9. Rass K, Reichrath J. UV damage and DNA repair in malignant melanoma and nonmelanoma skin cancer. Adv. Exp. Med. Biol. 2008; 624:162–178. [PubMed: 18348455]
10. Gordon Spratt EA, Carucci JA. Skin cancer in immunosuppressed patients. Facial plastic surgery : FPS. 2013; 29:402–410. [PubMed: 24037934]
11. Schwarz T, Luger TA. Effect of UV irradiation on epidermal cell cytokine production. Journal of photochemistry and photobiology. B, Biology. 1989; 4:1–13.
12. Armstrong BK, Kricker A. The epidemiology of UV induced skin cancer. Journal of photochemistry and photobiology. B, Biology. 2001; 63:8–18.
13. Hayden CG, Cross SE, Anderson C, Saunders NA, Roberts MS. Sunscreen penetration of human skin and related keratinocyte toxicity after topical application. Skin Pharmacol. Physiol. 2005; 18:170–174. [PubMed: 15908756]
14. Quatrano NA, Dinulos JG. Current principles of sunscreen use in children. Curr. Opin. Pediatr. 2013; 25:122–129. [PubMed: 23295720]
15. Liu X, et al. Hair follicles contribute significantly to penetration through human skin only at times soon after application as a solvent deposited solid in man. Br. J. Clin. Pharmacol. 2011; 72:768–774. [PubMed: 21599723]
16. Gulston M, Knowland J. Illumination of human keratinocytes in the presence of the sunscreen ingredient Padimate-O and through an SPF-15 sunscreen reduces direct photodamage to DNA but increases strand breaks. Mutat Res-Gen Tox En. 1999; 444:49–60.
17. Bastien N, Millau JF, Rouabhia M, Davies RJ, Drouin R. The sunscreen agent 2-phenylbenzimidazole-5-sulfonic acid photosensitizes the formation of oxidized guanines in cellulo after UV-A or UV-B exposure. The Journal of investigative dermatology. 2010; 130:2463–2471. [PubMed: 20574440]
18. Krause M, et al. Sunscreens: are they beneficial for health? An overview of endocrine disrupting properties of UV-filters. Int. J. Androl. 2012; 35:424–436. [PubMed: 22612478]
19. Hayden CGJ, Roberts MS, Benson HAE. Systemic absorption of sunscreen after topical application. Lancet. 1997; 350:863–864. [PubMed: 9310609]
20. Barnard AS. One-to-one comparison of sunscreen efficacy, aesthetics and potential nanotoxicity. Nature nanotechnology. 2010; 5:271–274.

21. Leite-Silva VR, et al. The effect of formulation on the penetration of coated and uncoated zinc oxide nanoparticles into the viable epidermis of human skin in vivo. Eur. J. Pharm. Biopharm. 2013; 84:297–308. [PubMed: 23454052]
22. Pan Z, et al. Adverse Effects of Titanium Dioxide Nanoparticles on Human Dermal Fibroblasts and How to Protect Cells. Small. 2009; 5:511–520. [PubMed: 19197964]
23. Trouiller B, Reliene R, Westbrook A, Solaimani P, Schiestl RH. Titanium dioxide nanoparticles induce DNA damage and genetic instability in vivo in mice. Cancer Res. 2009; 69:8784–8789. [PubMed: 19887611]
24. Wu J, et al. Toxicity and penetration of TiO2 nanoparticles in hairless mice and porcine skin after subchronic dermal exposure. Toxicology letters. 2009; 191:1–8. [PubMed: 19501137]
25. Zhang H, Shan Y, Dong L. A comparison of TiO2 and ZnO nanoparticles as photosensitizers in photodynamic therapy for cancer. Journal of biomedical nanotechnology. 2014; 10:1450–1457. [PubMed: 25016645]
26. Planta MB. Sunscreen and melanoma: is our prevention message correct? Journal of the American Board of Family Medicine : JABFM. 2011; 24:735–739. [PubMed: 22086817]
27. Lindqvist PG, et al. Avoidance of sun exposure is a risk factor for all-cause mortality: results from the Melanoma in Southern Sweden cohort. J. Intern. Med. 2014; 276:77–86. [PubMed: 24697969]
28. Plourde, E. Sunscreens - Biohazard: Treat As Hazardous Waste. New Voice Publications; 2011.
29. Kimura E, Kawano Y, Todo H, Ikarashi Y, Sugibayashi K. Measurement of skin permeation/penetration of nanoparticles for their safety evaluation. Biol. Pharm. Bull. 2012; 35:1476–1486. [PubMed: 22975498]
30. Vogt A, et al. 40 nm, but not 750 or 1,500 nm, nanoparticles enter epidermal CD1a+ cells after transcutaneous application on human skin. J. Investig. Dermatol. 2006; 126:1316–1322. [PubMed: 16614727]
31. Mitragotri S, Burke PA, Langer R. Overcoming the challenges in administering biopharmaceuticals: formulation and delivery strategies. Nature reviews. Drug discovery. 2014; 13:655–672. [PubMed: 25103255]
32. Gu H, Roy K. Topical permeation enhancers efficiently deliver polymer micro and nanoparticles to epidermal Langerhans' cells. J Drug Deliv Sci Tec. 2004; 14:265–273.
33. Deng Y, et al. The effect of hyperbranched polyglycerol coatings on drug delivery using degradable polymer nanoparticles. Biomaterials. 2014; 35:6595–6602. [PubMed: 24816286]
34. Thavarajah R, Mudimbaimannar VK, Elizabeth J, Rao UK, Ranganathan K. Chemical and physical basics of routine formaldehyde fixation. Journal of oral and maxillofacial pathology : JOMFP. 2012; 16:400–405. [PubMed: 23248474]
35. Sompuram SR, Vani K, Messana E, Bogen SA. A molecular mechanism of formalin fixation and antigen retrieval. Am. J. Clin. Pathol. 2004; 121:190–199. [PubMed: 14983931]
36. Zhu H, et al. Global analysis of protein activities using proteome chips. Science. 2001; 293:2101–2105. [PubMed: 11474067]
37. Artzi N, Shazly T, Baker AB, Bon A, Edelman ER. Aldehyde-amine chemistry enables modulated biosealants with tissue-specific adhesion. Advanced materials. 2009; 21:3399–3403. [PubMed: 20882504]
38. Gu F, et al. Precise engineering of targeted nanoparticles by using self-assembled biointegrated block copolymers. Proc. Natl. Acad. Sci. U. S. A. 2008; 105:2586–2591. [PubMed: 18272481]
39. Rao SS, Han N, Winter JO. Polylysine-modified PEG-based hydrogels to enhance the neuro-electrode interface. J. Biomater. Sci. Polym. Ed. 2011; 22:611–625. [PubMed: 20566048]
40. Swindle MM, Makin A, Herron AJ, Clubb FJ, Frazier KS. Swine as models in biomedical research and toxicology testing (vol 49, pg 344, 2012). Veterinary Pathology. 2012; 49:738–738.
41. Barbero AM, Frasch HF. Pig and guinea pig skin as surrogates for human in vitro penetration studies: A quantitative review. Toxicol. In Vitro. 2009; 23:1–13. [PubMed: 19013230]
42. Downes AM, Matoltsy AG, Sweeney TM. Rate of turnover of the stratum corneum in hairless mice. The Journal of investigative dermatology. 1967; 49:400–405. [PubMed: 6058500]

43. Nair HB, Ford A, Dick EJ Jr, Hill RH Jr, VandeBerg JL. Modeling sunscreen-mediated melanoma prevention in the laboratory opossum (Monodelphis domestica). Pigment cell & melanoma research. 2014; 27:843–845. [PubMed: 24931873]
44. Bennassar A, Grimalt R, Romaguera C, Vilaplana J. Two cases of photocontact allergy to the new sun filter octocrylene. Dermatology online journal. 2009; 15:14. [PubMed: 20040264]
45. Rietschel, RL. Fisher's Contact Dermatitis. 6 edition. Pmph Usa: 2007 Apr 2.
46. Andreas Katsambas, TL. European Handbook of Dermatological Treatments. Berlin Heidelberg: Springer-Verlag; 2003.
47. Flick, EW. Cosmetic and Toiletry Formulations. Noyes Publications; 1984.
48. Tanner PR. Sunscreen product formulation. Dermatologic clinics. 2006; 24:53-+. [PubMed: 16311167]
49. Egerton TA. UV-absorption--the primary process in photocatalysis and some practical consequences. Molecules. 2014; 19:18192–18214. [PubMed: 25383755]
50. Perugini P, et al. Effect of nanoparticle encapsulation on the photostability of the sunscreen agent, 2-ethylhexyl-p-methoxycinnamate. International journal of pharmaceutics. 2002; 246:37–45. [PubMed: 12270607]
51. Matsumura Y, Ananthaswamy HN. Toxic effects of ultraviolet radiation on the skin. Toxicol. Appl. Pharmacol. 2004; 195:298–308. [PubMed: 15020192]
52. Han J, Colditz GA, Samson LD, Hunter DJ. Polymorphisms in DNA double-strand break repair genes and skin cancer risk. Cancer Res. 2004; 64:3009–3013. [PubMed: 15126335]
53. Rogakou EP, Pilch DR, Orr AH, Ivanova VS, Bonner WM. DNA double-stranded breaks induce histone H2AX phosphorylation on serine 139. J. Biol. Chem. 1998; 273:5858–5868. [PubMed: 9488723]
54. Deng Y, Zhu XY, Kienlen T, Guo A. Transport at the air/water interface is the reason for rings in protein microarrays. J. Am. Chem. Soc. 2006; 128:2768–2769. [PubMed: 16506733]
55. Deng Y, et al. Global analysis of human nonreceptor tyrosine kinase specificity using high-density Peptide microarrays. J. Proteome Res. 2014; 13:4339–4346. [PubMed: 25164267]

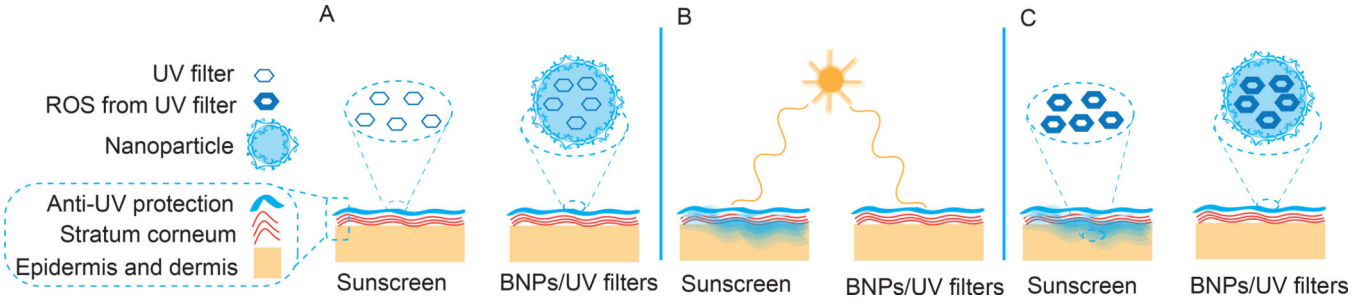

Figure 1. Comparison of BNP based sunscreen to commercial sunscreen

(A) Sunscreen formulations are applied onto the skin. (B) After application, commercial sunscreen penetrates into the skin whereas the BNP formulation remains on the stratum corneum. (C) After sunlight exposure, UV filters produce deleterious ROS which can damage adjacent tissue, however, BNPs do not penetrate into the skin and prevent ROS mediated toxicity by confining these toxic products within the particle. BNP - bioadhesive nanoparticle, ROS - reactive oxygen species, UV – ultraviolet.

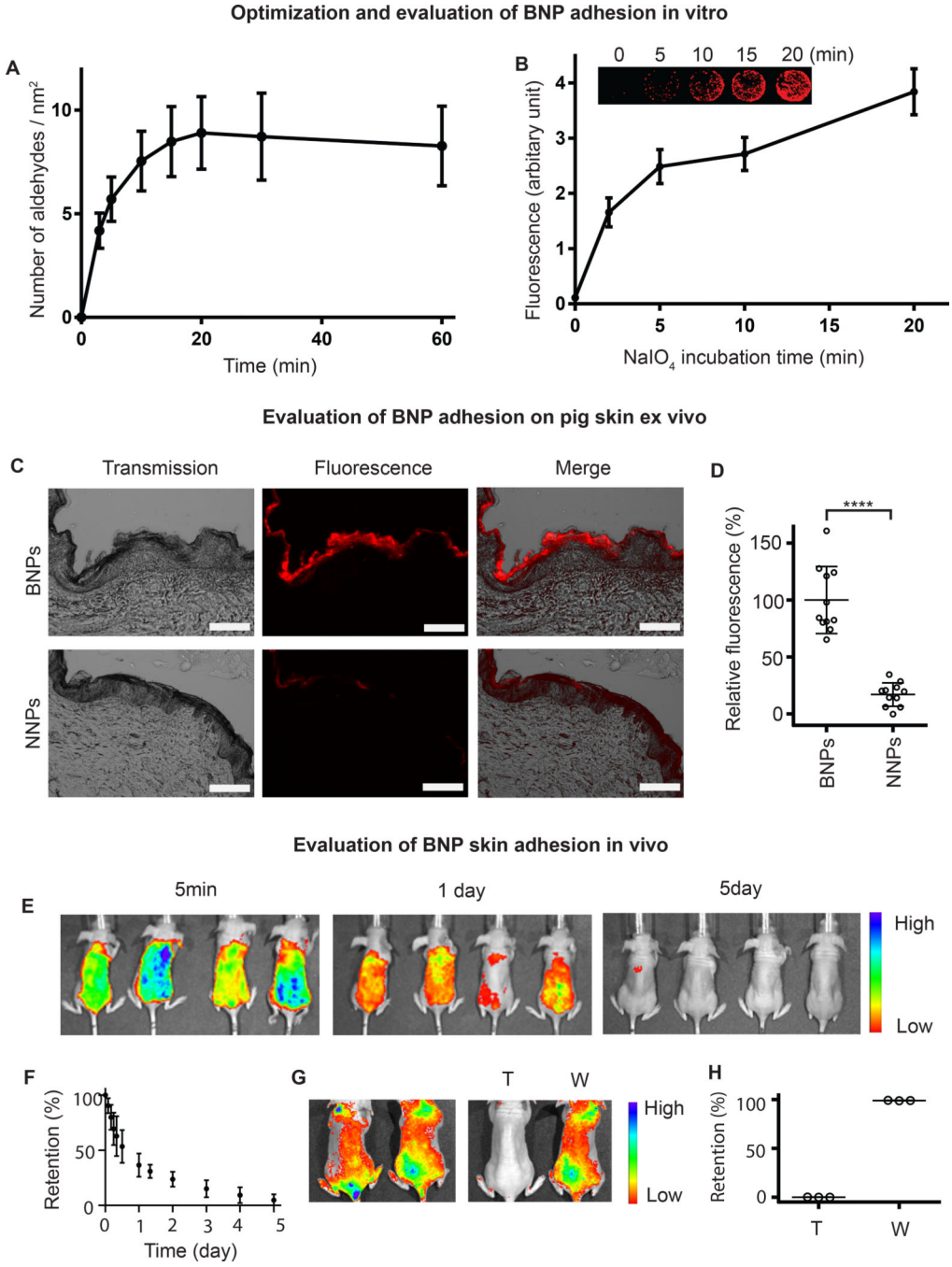

Figure 2. Evaluation of BNP adhesion

(A) Surface aldehyde concentration on nanoparticles were recorded as a function of incubation time with NaIO4. Data are shown as mean ± SD (n = 4). (B) Surface immobilization of BNPs on lysine coated slides. The surface density of aldehydes was controlled by incubation time with NaIO4. The non-treated group (0 min) represent NNPs (non-adhesive control). Data are shown as mean ± SD (n = 4). (C) BNPs and NNPs at 1 mg/ml were incubated on pig skin for six hours in a humidity chamber at 32°C. The scale bar represents 200 μm. (D) The fluorescence was quantified and normalized to the average

fluorescence of BNPs. Data are shown as mean ± SD (n = 10), ****P < 0.0001 (student t-test). (E) BNPs encapsulating an infrared dye, IR-780, were applied on dorsal skin of mice and BNP skin retention was imaged with Xenogen at different time points. (F) The fluorescence was quantified and normalized to the fluorescence intensity at time zero. (G) BNPs encapsulating an infrared dye, IR-780, were applied to the dorsal skin of mice. After wiping with a wet towel (T) or washing with water (W), BNP skin retention was imaged with Xenogen. (H) The fluorescence after wiping or washing was quantified and normalized to the fluorescence intensity at time zero. BNP - bioadhesive nanoparticle, NNP - non-bioadhesive nanoparticles.

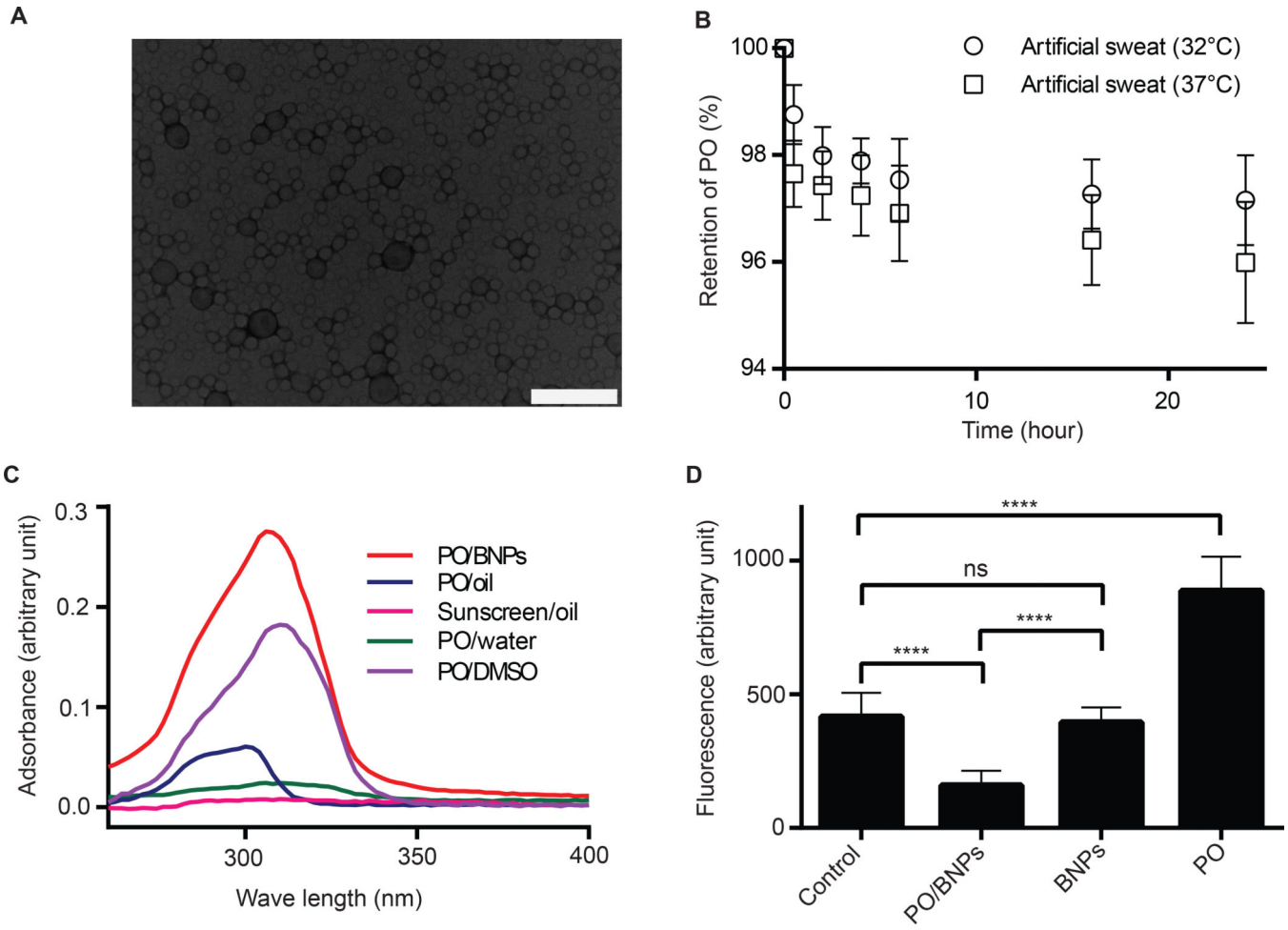

Figure 3. Synthesis and *in vitro* evaluation of PO/BNPs

(A) TEM image of PO/BNPs. The scale bar is 200 nm. (B) PO retention within PO/BNPs in artificial human sweat at 32°C and 37°C. Data are shown as mean ± SD (n = 4). (C) Absorbance efficiency of PO/BNPs, PO emulsion in water (PO/water), PO dissolved in mineral oil (PO/Oil), PO dissolved in DMSO (PO/DMSO) at a PO concentration of 0.01 mg/ml, and sunscreen dissolved in mineral oil (Sunscreen/Oil) at 0.01 mg/ml of active ingredients. UV filters within their vehicles were scanned for UV absorbance between 260–400nm. The data are plotted with background subtraction of blank vehicles. Data are shown as mean (n=4). (D) ROS formation as measured by DHR fluorescence after UV irradiation. DHR was incubated with PO/BNPs, blank BNPs, PO emulsion and PBS control. Data are shown as mean ± SD (n = 8), ****P<0.0001. BNP - bioadhesive nanoparticle, DHR – Dihydrorhodamine, DMSO - dimethyl sulfoxide, PO – padimate O, ROS – reactive oxygen species, TEM - transmission electron microscopy, UV – ultraviolet.

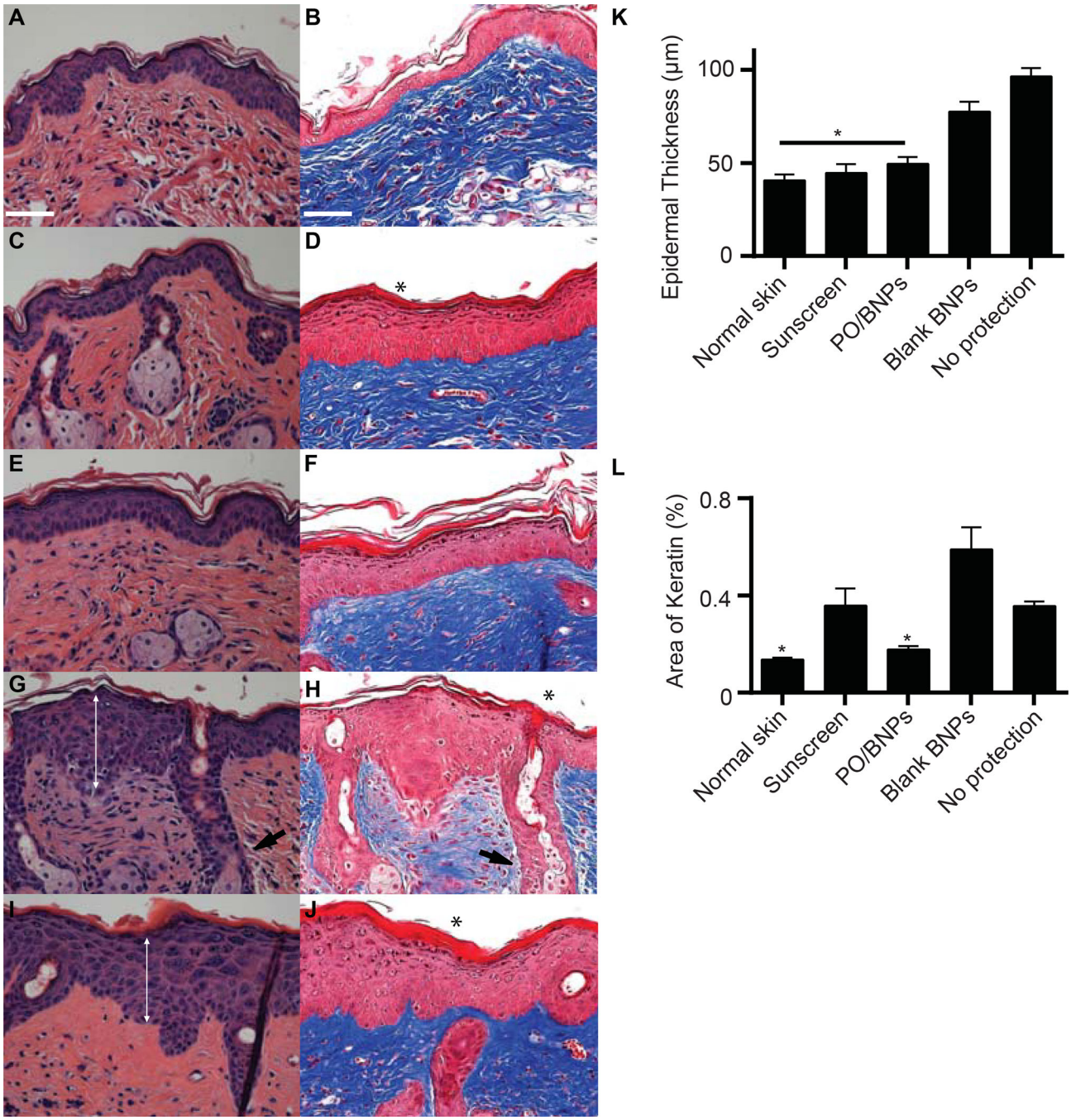

Figure 4. Histology of dorsal mouse skin sections receiving different topical interventions three days after high dose UV (2160 J/m^2)

Topical interventions included (A–B) normal skin without UV exposure, (C–D) sunscreen, (E–F) PO/BNPs, (G–H) blank BNPs, (I–J) no protection. There was significant acanthosis (double arrow) with prominent rete ridges (arrow) and orthokeratosis (*) present in the unprotected samples, consistent with epidermal hypertrophy. Skin protected by sunscreen showed thickened orthokeratosis as well relative to the skin protected by PO/BNPs and the normal skin control. (K) Epidermal thickness and (L) percent area of keratin within the dorsal skin after receiving topical interventions and UV irradiation. The scale bar represents

100 μm. Hematoxylin and eosin staining (A, C, E, G, I). Trichrome staining (B, D, F, H, J). *$p<0.05$ compared to all other treatment groups. BNP - bioadhesive nanoparticle, PO – padimate O.

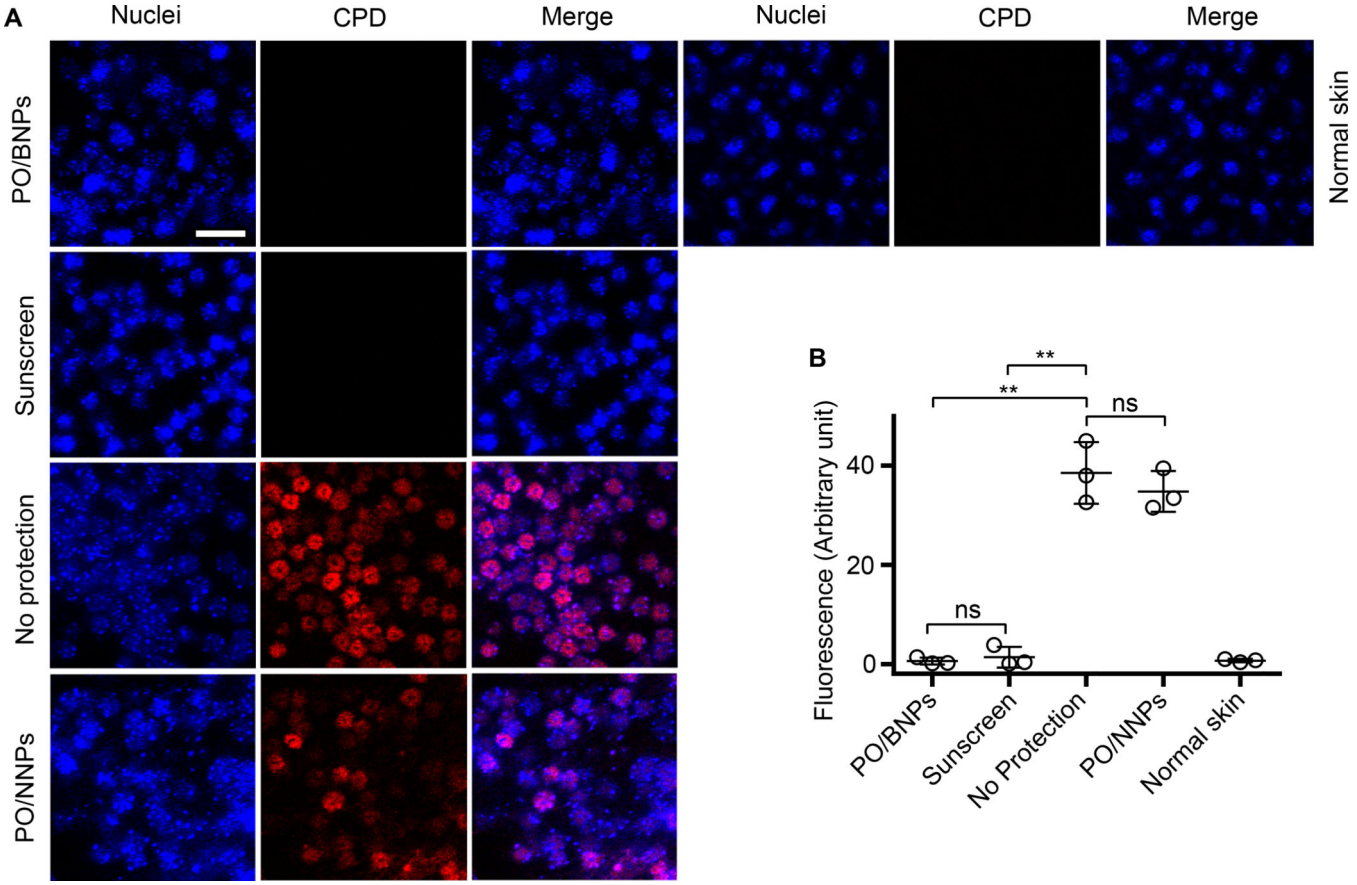

Figure 5. CPD staining of mouse dorsal epidermal sheets after receiving different topical interventions and UVB irradiation (160 J/m^2)

Epidermal sheets were prepared one hour after exposure to UVB (A). The fluorescence of CPD on skin receiving different topical interventions was quantified (B). The scale bar represents 50 μm. Data are shown as mean ± SD (n=3), **p<0.01 (student t-test). Normal skin represents tissue that was not UV irradiated. BNP - bioadhesive nanoparticle, CPD - cyclobutane pyrimidine dimers, PO – padimate O.

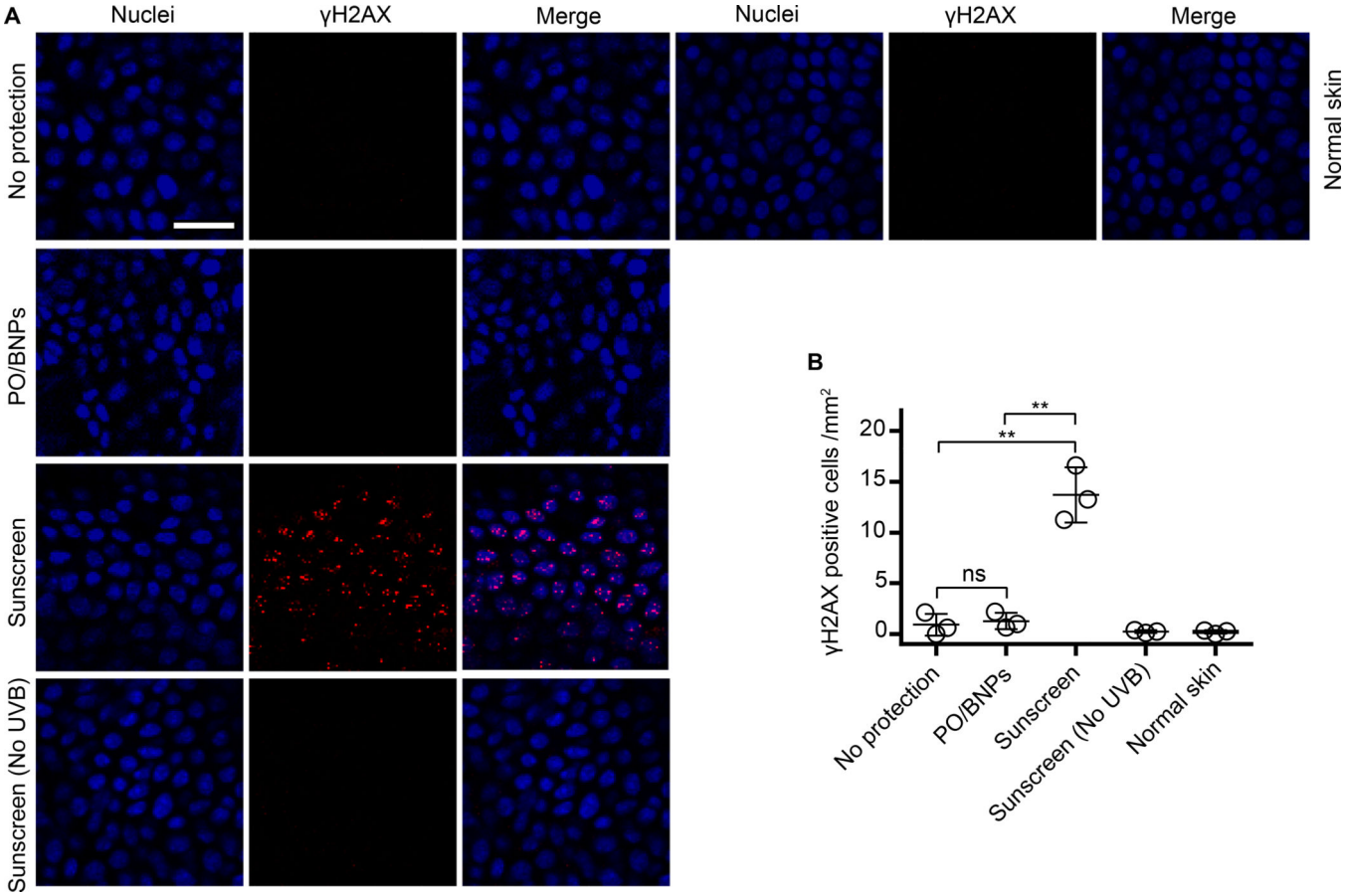

Figure 6. Staining for γH2AX on mouse dorsal epidermal sheets receiving different topical interventions and UVB irradiation (160 J/m^2)

(A) Epidermal sheets were prepared 20 hours after exposure to UV-B. (B) The γH2AX+ cells within the epidermis for each intervention were enumerated. The scale bar represents 50 μm. Data are shown as mean ± SD (n=3), **p ≤ 0.01 (student t-test). Normal skin represents tissue that was not UV irradiated. γH2AX – phosphorylated histone H2A variant H2AX, BNP - bioadhesive nanoparticle, NS – not significant, PO – padimate O, UV – ultraviolet.